Technical University of Denmark

DTU

Self-consistent tight-binding model of B and N doping in graphene

Pedersen, Thomas Garm; Pedersen, Jesper Goor

DTU Library
Technical Information Center of Denmark

Self-consistent tight-binding model of B and N doping in graphene

Thomas Garm Pedersen[1,2] and Jesper Goor Pedersen[3]

[1]*Department of Physics and Nanotechnology, Aalborg University, DK-9220 Aalborg Øst, Denmark*
[2]*Center for Nanostructured Graphene (CNG), DK-9220 Aalborg Øst, Denmark*
[3]*DTU Nanotech, Technical University of Denmark, DK-2800 Kongens Lyngby, Denmark*

Boron and nitrogen substitutional impurities in graphene are analyzed using a self-consistent tight-binding approach. An analytical result for the impurity Green's function is derived taking broken electron-hole symmetry into account and validated by comparison to numerical diagonalization. The impurity potential depends sensitively on the impurity occupancy, leading to a self-consistency requirement. We solve this problem using the impurity Green's function and determine the self-consistent local density of states at the impurity site and, thereby, identify acceptor and donor energy resonances.

I. INTRODUCTION

Control over carrier densities is essential for realization of graphene-based electronic, plasmonic, opto-electronic, and transparent conductive devices.[1–3] Intrinsic carrier mobilities in graphene are exceptionally high,[4] and carriers can be supplied either actively via gating[4,5] or passively via chemical doping.[6–9] Particular attention has been paid to chemical doping via substitutional impurities such as boron and nitrogen providing p- and n-type doping, respectively. These species are found to be readily accommodated by the graphene lattice,[9,10] thus paving the way for practical devices.

In the simplest theoretical model of graphene doping, such impurities simply enter via a fixed donor or acceptor level, similar to the case of gapped semiconductors. Realistically, however, for a metallic or semimetallic material, impurity levels are coupled to the entire continuum of bulk states, and a much more accurate picture may be provided by the energy-dependent local density of electronic states at the impurity sites. Donor or acceptor levels may subsequently be identified as resonances in the local density of states. Several publications have investigated this problem at *ab initio*[11–13] and tight-binding[13–21] levels. The tight-binding approach is obviously highly suited for analysis of localized impurity states. Moreover, the long-range nature of impurity-impurity interactions requires rather large simulation cells, making first-principles calculations challenging.[12,13] A simple, orthogonal nearest-neighbor tight-binding model is capable of qualitatively modeling several impurity-related properties.[15,16,18] The implicit assumptions, such as perfect electron-hole symmetry, are problematic, however. This deficiency may be partly relieved by the inclusion of next-nearest-neighbor terms[17] or overlap corrections.[19] Finite overlap corrections may also be implemented for adsorbate interactions with graphene.[20] Equally questionable is the choice of tight-binding parameters. In particular, the precise value of the impurity potential is crucial for the predicted properties. Therefore, this parameter is often treated as an adjustable variable. In fact, a single, fixed value is unlikely to capture the correct behavior because the impurity potential depends in a sensitive manner on the electron occupation *n* at the impurity site. In the self-consistent charge tight-binding approach, the *n*-dependence of the impurity potential is linearized around the neutral-atom value with the slope identified as the Hubbard *U*-parameter.[22]

Hence, with this extension of the tight-binding approach, an accurate impurity potential can be found from a self-consistent solution of the electronic problem.

In this paper, we adopt a self-consistent tight-binding approach to N- and B-doping in graphene. The density-functional–based approach to computation of tight-binding parameters (DFTB) has previously been successfully applied to graphene nanostructures,[23–25] and we apply this method for all on-site parameters. Moreover, nonorthogonality between neighbor orbitals is retained via a nonvanishing overlap integral. This ensures broken electron-hole symmetry in agreement with first-principles results. The presence of nonorthogonality complicates slightly the impurity Green's function, but we demonstrate that relatively simple analytical expressions can be derived in terms of the result for the orthogonal case. We then apply this Green's function to solve the self-consistency issue. Our strategy is to combine results for the impurity occupancy derived by integrating the local density of states with the general occupancy-dependent impurity on-site energy. In this manner, unique B- and N-impurity potentials are determined. In turn, this allows us to identify acceptor and donor resonance energies.

II. SELF-CONSISTENT TIGHT-BINDING MODEL

In our model, we assume an infinite graphene sheet, in which a single atom has been substituted by an impurity, forming so-called graphitic impurities. The perturbed π states are found as eigenstates of a Hamiltonian $\boldsymbol{H} = \boldsymbol{H}_0 + \boldsymbol{H}_1$ with

$$\boldsymbol{H}_0 = \sum_i \varepsilon_p \, |i\rangle \, \langle i| - \sum_{i,j} t_{ij} \, |i\rangle \, \langle j|, \quad \boldsymbol{H}_1 = \Delta \, |1\rangle \, \langle 1|. \quad (1)$$

Here, ε_p is the carbon on-site energy, and the last term in $\boldsymbol{H}_0$ describes hopping between sites i and j with hopping integral t_{ij}. The sum generally covers all pairs of different sites, but in order to find an analytical solution, we limit the sum to nearest neighbors. The added part $\boldsymbol{H}_1$ is the impurity Hamiltonian taking $|1\rangle$ as the impurity site. Hence, the total impurity on-site energy is $\varepsilon_p + \Delta$. The value of the hopping integral t_{ij} depends on the atomic species forming the bond and, hence, differs from the bulk value around the impurity. We will ignore this complication, however, and use the bulk graphene value $t_{ij} \equiv t \approx 3\text{eV}$ in all cases.[26]
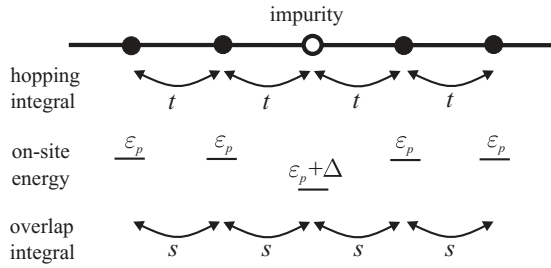
FIG. 1. Schematic illustration of the impurity model assuming identical hopping and overlap integrals between all nearest neighbors.

Finally, we do *not* make the usual assumption of orthogonal neighbor π states. The value of the overlap $s = \langle i \mid j \rangle$ for i and j nearest neighbors differs between various tight-binding parameterizations, with common choices being $s = 0.129$ (Ref. 26) up to as high as $s = 0.267$ (Ref. 27). Below, we vary s between 0 and 0.15 (regarding $s \approx 0.15$ as the physically realistic value), and, as will be demonstrated, this correction has a very significant impact on impurity resonance energies. In DFTB, the computed values of s at a separation of 1.42 Å are 0.149 and 0.130 for C-C and C-N pairs, respectively. The inaccuracy of assuming identical values of s can therefore be estimated as roughly 13%. For the hopping integrals, the corresponding number is as small as 4%. Hence, the proposed model corresponds schematically to the picture in Fig. 1. Since identical hopping and overlap integrals are assumed for all nearest neighbors, the nature of the impurity is determined entirely through the impurity potential Δ.

The on-site energies obviously play a crucial role in the problem. A general on-site energy ε depends on the electron occupancy of the atom n so that $\varepsilon = \varepsilon(n)$,[22,28] where $0 \leqslant n \leqslant 2$. In practice, we will apply the linearized relation

$$\varepsilon \approx \varepsilon_0 + U \cdot (n - n_0), \qquad (2)$$

where ε_0 is the neutral-atom value, U is the Hubbard U parameter, and n_0 is the electron occupancy of a neutral atom. In all cases considered here (B, C, and N), three valence electrons are assumed given up to the σ bond network. Hence, n_0 is 0, 1, and 2 for the three species, respectively. In the spirit of density-functional–based tight-binding, the remaining parameters ε_0 and U are found from a density-functional calculation of the $2p$ atomic eigenvalue and the numerical derivative of the eigenvalue with respect to electron number, respectively.[28] We apply the local density approximation in the Perdew-Zunger parameterization[29] without spin-polarization, yielding the results shown in Table I. We thus take $\varepsilon_P = -5.43$ eV. The Hubbard U parameters determine the energetic cost of occupying the impurity. In this connection, we note that by assuming a purely local interaction derived for an isolated atom and, accordingly, ignoring electron-electron interactions

TABLE I. Atomic on-site parameters.

Atom	On-site energy ε_0 (eV)	Hubbard U (eV)
B	-3.74	7.8
C	-5.43	9.7
N	-7.25	11.5

with neighbor sites, we may overestimate the Coulomb correction. In fact, Schlüter *et al.*[30] find that nonlocal interactions reduce the effective Hubbard U by about 50%. Below, we therefore consider both isolated-atom and effective U values in the numerical evaluations. Note, that the dependence of on-site energies on electron occupation constitutes a self-consistency problem. Since electron occupation is a sensitive function of on-site energies, we generally need an iterative approach. Starting from an initial value of n, the electron occupancy is repeatedly updated via the charge computed using the corresponding on-site values until convergence is reached. Below, we will show how an analytic approach is able to bypass this obstacle.

The present nonorthogonal tight-binding model can be solved numerically as a generalized eigenvalue problem for large but finite geometries. By duplicating the original graphene unit cell, we construct an N by N supercell containing $2N^2$ atoms, among which one is the impurity. We use periodic boundary conditions to eliminate finite-size effects in the results. Note, however, that interactions among impurities in neighboring supercells will affect the results if N is not sufficiently large.[12,13] The resulting matrix problem reads $(\boldsymbol{H}_0 + \boldsymbol{H}_1) \cdot \boldsymbol{c}_{n,\vec{k}} = E_{n,\vec{k}} \boldsymbol{S} \cdot \boldsymbol{c}_{n,\vec{k}}$, where n and $\vec{k}$ label band and k-vector, respectively, $\boldsymbol{S}$ is the overlap matrix, and $E_{n,\vec{k}}$ and $\boldsymbol{c}_{n,\vec{k}}$ denote eigenvalues and eigenvectors. If a total of $N_{\vec{k}}$ k-points in the irreducible Brillouin zone are sampled, the local density of states $L(\omega)$ on the impurity site is evaluated numerically as

$$L(\omega) = \frac{1}{N_{\vec{k}}} \sum_{n,\vec{k}} \rho_{n,\vec{k}}^{(1)} \delta(\omega - E_{n,\vec{k}}),$$

$$\rho_{n,\vec{k}}^{(i)} = \text{Re}\left\{ \boldsymbol{c}_{n,\vec{k}}^{(i)*} \sum_j \boldsymbol{S}_{ij} \boldsymbol{c}_{n,\vec{k}}^{(j)} \right\}, \qquad (3)$$

where ω is the energy. The expression for the weight $\rho_{n,\vec{k}}^{(i)}$ differs from the standard result in that overlap corrections are accounted for.[22] Eventually, assuming zero temperature conditions, the impurity electron occupancy is found by integrating $L(\omega)$ below the Fermi level E_F.

III. ANALYTICAL GREEN'S FUNCTION APPROACH

While the numerical diagonalization method is accurate for sufficiently large supercells, it is necessarily rather computationally demanding. It is possible to accelerate this approach using recursive Green's function methods,[13,18] even though complications arise from the presence of the overlap matrix. Here, we will demonstrate, however, that the problem can be solved analytically via the Dyson equation. We will show that knowledge of the solution for the standard, orthogonal problem can be adapted to tackle the present, nonorthogonal problem. This analytical approach greatly simplifies the subsequent analysis and allows for a simple solution of the self-consistency relations.

The analytical approach revolves around the retarded Green's function $\boldsymbol{G}(\omega)$, which provides the local density of states $L(\omega)$ via $L(\omega) = -\pi^{-1}\text{Im}\boldsymbol{G}_{11}(\omega)$, where $\boldsymbol{G}_{11}(\omega)$ is the diagonal element associated with the impurity site. Formally, any nonorthogonal model $\boldsymbol{H} \cdot \boldsymbol{c} = E\boldsymbol{S} \cdot \boldsymbol{c}$ is readily converted

to a standard one simply by inverting the overlap matrix, i.e., $(\boldsymbol{S}^{-1}\boldsymbol{H}) \cdot \boldsymbol{c} = E\boldsymbol{c}$. Therefore, the Green's function of the nonorthogonal model must be defined as

$$\boldsymbol{G}(z) = (z - \boldsymbol{S}^{-1}\boldsymbol{H})^{-1} = (z\boldsymbol{S} - \boldsymbol{H})^{-1}\,\boldsymbol{S} \equiv \tilde{\boldsymbol{G}}(z)\boldsymbol{S}. \quad (4)$$

For the impurity model with $\boldsymbol{H} = \boldsymbol{H}_0 + \boldsymbol{H}_1$, the unperturbed Green's functions are consequently defined as

$$\boldsymbol{G}_0(z) = (z - \boldsymbol{S}^{-1}\boldsymbol{H}_0)^{-1}, \quad \tilde{\boldsymbol{G}}_0(z) = (z\boldsymbol{S} - \boldsymbol{H}_0)^{-1}. \quad (5)$$

In this "standard" picture, the perturbation is $\boldsymbol{S}^{-1}\boldsymbol{H}_1$, and so the Dyson equation becomes

$$\boldsymbol{G}(z) = \boldsymbol{G}_0(z) + \boldsymbol{G}_0(z)\boldsymbol{S}^{-1}\boldsymbol{H}_1\boldsymbol{G}(z). \quad (6)$$

As $\tilde{\boldsymbol{G}}_0(z) = \boldsymbol{G}_0(z)\boldsymbol{S}^{-1}$, we have $\boldsymbol{G}(z) = (1 - \tilde{\boldsymbol{G}}_0(z)\boldsymbol{H}_1)^{-1}$ $\boldsymbol{G}_0(z)$, and with a local perturbation

$$G_{11}(z) = \frac{G_{11}^0(z)}{1 - \Delta \tilde{G}_{11}^0(z)}. \quad (7)$$

This relation demonstrates that a nonorthogonal model leads to the necessity of treating two separate unperturbed Green's functions $\boldsymbol{G}_0(z)$ and $\tilde{\boldsymbol{G}}_0(z) = \boldsymbol{G}_0(z)\boldsymbol{S}^{-1}$. For the specific case of graphene, we will now discuss how these are obtained.

In the usual description of π states in the two-atomic unit cell of graphene, the assumption of nearest-neighbor hopping and overlap interactions yields the matrices

$$\boldsymbol{H}_0 = \begin{pmatrix} \varepsilon_p & -th \\ -th^* & \varepsilon_p \end{pmatrix}, \quad \boldsymbol{S} = \begin{pmatrix} 1 & sh \\ sh^* & 1 \end{pmatrix}, \quad (8)$$

where $h = 1 + 2\cos\left(\frac{1}{2}k_y a\right)\exp\left(\frac{i\sqrt{3}}{2}k_x a\right)$ is the sum of nearest-neighbor Bloch phases with a defined as the graphene lattice constant. Now, the fact that h enters in the off-diagonal elements of both matrices means that we can apply a previously used trick to reformulate the problem.[31,32] By transferring the off-diagonal elements of $\boldsymbol{S}$ to the left-hand side, the generalized eigenvalue problem $\boldsymbol{H}_0 \cdot \boldsymbol{c}_{n,\vec{k}} = E_{n,\vec{k}}\boldsymbol{S} \cdot \boldsymbol{c}_{n,\vec{k}}$ is transformed into a standard one, $\boldsymbol{h}_0 \cdot \boldsymbol{c}_{n,\vec{k}} = \varepsilon_{n,\vec{k}}\boldsymbol{c}_{n,\vec{k}}$, with the relations

$$\boldsymbol{h}_0 = \begin{pmatrix} 0 & -th \\ -th^* & 0 \end{pmatrix}, \quad E_{n,\vec{k}} = \frac{\varepsilon_{n,\vec{k}} + \varepsilon_p}{1 - \varepsilon_{n,\vec{k}}\frac{s}{t}}. \quad (9)$$

Using simple manipulations, it is then straightforward to demonstrate that

$$G_{11}^0(z) = \frac{1}{\Omega_{BZ}}\sum_n\int\frac{1}{z - E_{n,\vec{k}}}d^2k$$

$$= \frac{1}{1 + z\frac{s}{t}} \cdot \frac{1}{\Omega_{BZ}}\sum_n\int\frac{1 - \varepsilon_{n,\vec{k}}\frac{s}{t}}{\frac{z - \varepsilon_p}{1 + z\frac{s}{t}} - \varepsilon_{n,\vec{k}}}d^2k, \quad (10)$$

where Ω_{BZ} is the Brillouin zone area. If we next introduce the Green's function of the standard problem

$$g_0(z) = \frac{1}{\Omega_{BZ}}\sum_n\int\frac{1}{z - \varepsilon_{n,\vec{k}}}d^2k, \quad (11)$$

we find

$$G_{11}^0(z) = \frac{1 + \varepsilon_p\frac{s}{t}}{\left(1 + z\frac{s}{t}\right)^2}g_0\left(\frac{z - \varepsilon_p}{1 + z\frac{s}{t}}\right) + \frac{s}{t + zs}. \quad (12)$$
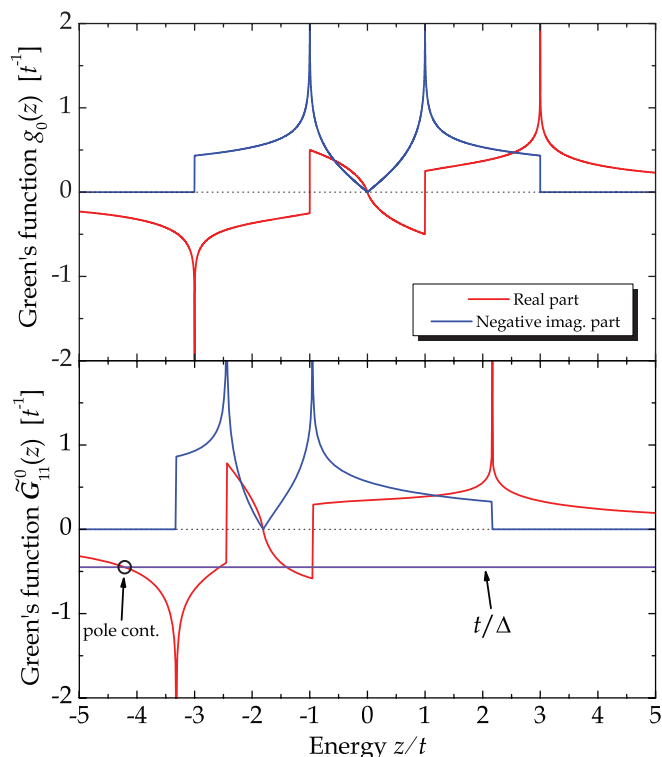
FIG. 2. (Color online) Green's function of the orthogonal (upper panel) and nonorthogonal $s = 0.15$ (lower panel) models. In the lower panel, the circle indicates the pole contribution to the impurity occupancy.

Moreover,

$$\tilde{G}_{11}^0(z) = \frac{1}{1 + z\frac{s}{t}}g_0\left(\frac{z - \varepsilon_p}{1 + z\frac{s}{t}}\right). \quad (13)$$

Thus, the required Green's functions of the nonorthogonal problem follow directly from the solution to the standard orthogonal case. This problem has been studied in detail previously,[33] and the result can be written as[34]

$$g_0(z) = \text{sign}(z)\text{Re}\{3\mathcal{G}(|z|) + \mathcal{G}(-|z|)\}$$
$$\qquad + i\text{Im}\{\mathcal{G}(|z|) - \mathcal{G}(-|z|)\},$$
$$\mathcal{G}(z) = \frac{\sqrt{z}}{2\pi i t^{3/2}}K\left[\frac{(3t - z)(t + z)^3}{16zt^3}\right], \quad (14)$$

where the Mathematica definition of the complete elliptic integrals $K(x) = \int_0^{\pi/2}\left(1 - x\sin^2\theta\right)^{-1/2}d\theta$ is applied. The standard and modified Green's functions for $s = 0.15$ are shown in Fig. 2. The functions differ in two obvious ways: a (trivial) shift due to the nonvanishing ε_p and a clearly broken electron-hole symmetry due to the nonvanishing overlap s.

IV. RESULTS

To verify the main results from Eqs. (7), (12), and (13), we compare in Fig. 3 the local density of states computed using either numerical or analytical methods. We consider here a donor impurity problem and take $\Delta = -5$ eV as well as $s = 0.15$. The numerical result is obtained from the supercell approach described above using $N = 36$, i.e., a cell containing 2592 atoms. Moreover, we sample 5050 k-points
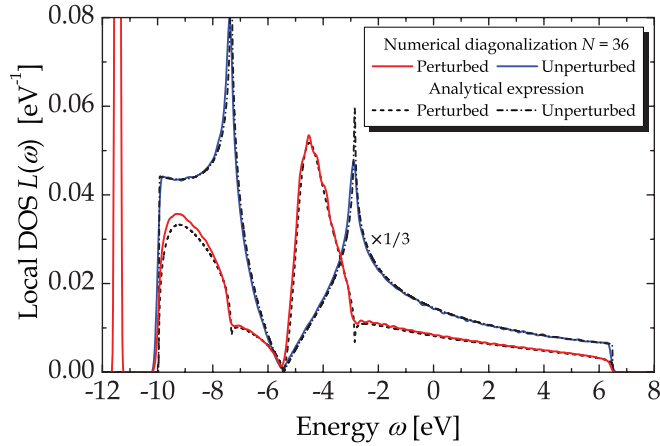
FIG. 3. (Color online) Energy dependence of the local density of states (DOS) computed by numerical diagonalization (solid lines) and analytically (dashed lines). Both perturbed ($\Delta = -5$ eV) and unperturbed ($\Delta = 0$) cases are shown.

FIG. 4. (Color online) Occupancy of an impurity versus potential Δ (blue curve). The straight lines are derived from the occupancy-dependent on-site potentials of N (red) and B (green) atoms, respectively. Both isolated-atom (full) and effective (dashed) Hubbard parameters are considered. The intersections correspond to self-consistent solutions.

in the irreducible wedge of the Brillouin zone. Such large supercells are required because of the long-range nature of impurity-impurity interactions.[13] While this is a rather demanding computation, the analytical formula provides an answer with very little computational effort. We note the excellent agreement between the two approaches. Note also, as discussed in detail below, that the numerical result includes the pole contribution around -11.4 eV, which is absent in the analytical counterpart, as we only plot the regular (principal value) part. Hence, this example validates the developed method of computing the local density of states.

Next, we consider the electron occupancy of the impurity given by

$$n = -\pi^{-1} \int_{-\infty}^{E_F} \text{Im} \, \boldsymbol{G}_{11}(\omega) d\omega. \tag{15}$$

For a finite impurity density, the Fermi level E_F depends on the density. Here, very dilute doping and consequently low impurity density will be assumed, however. Hence, E_F coincides with ε_p throughout. Inspection of Eq.(7) demonstrates that there are two contributions to n. Primarily, $\boldsymbol{G}_0(\omega)$ and $\tilde{\boldsymbol{G}}_0(\omega)$ have finite imaginary parts in the energy range $\omega \in [\omega_-, \omega_+]$ with $\omega_\pm = (\varepsilon_p \pm 3t)/(1 \mp 3s)$. In addition, however, a pole contribution is found whenever $\Delta < 0$. From Eq. (7), it follows that the pole location ω_0 is determined by the condition $1 - \Delta \tilde{\boldsymbol{G}}_{11}^0(\omega_0) = 0$. This point is indicated by the encircled intersection in the bottom panel of Fig. 2 and is responsible for the delta function–like contribution in the numerical results in Fig. 3. Hence, the total impurity occupancy is given by

$$n = -\pi^{-1} \int_{\omega_-}^{\varepsilon_p} \text{Im} \left\{ \frac{\boldsymbol{G}_{11}^0(\omega)}{1 - \Delta \tilde{\boldsymbol{G}}_{11}^0(\omega)} \right\} d\omega - \frac{\boldsymbol{G}_{11}^0(\omega_0)}{\Delta \partial \tilde{\boldsymbol{G}}_{11}^0 / \partial \omega |_{\omega = \omega_0}}. \tag{16}$$

For $\Delta > 0$, the pole condition still has a solution, but no contribution to n is obtained because $\omega_0 > E_F$ in this case. In this manner, we find the Δ dependence of the occupancy, as illustrated in Fig. 4. The central part near $\Delta = 0$ is excluded because of numerical instabilities in this range. Note that n
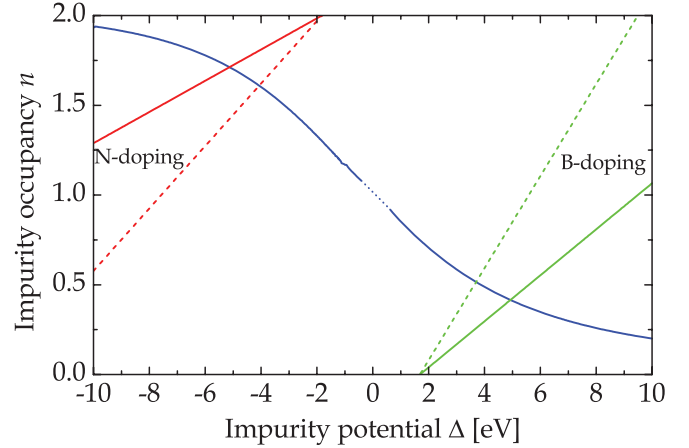
approaches 0 and 2 for high and low potentials, respectively, as expected.

We are now in a position to determine the actual self-consistent impurity potential for particular doping species. The impurity on-site energy is $\varepsilon = \varepsilon_p + \Delta$, and so Eq. (2) can be recast as

$$n = \frac{\varepsilon_p + \Delta - \varepsilon_0 + U n_0}{U}. \tag{17}$$

This linear dependence on Δ is included as the straight lines in Fig. 4 for N-doping (red lines) and B-doping (green lines), respectively, using the parameters of Table I (full lines) as well as effective Hubbard parameters found by reducing the isolated-atom values by 50% [30] (dashed lines). It follows that the self-consistent impurity potentials can be determined simply as the intersections, and, in this manner, we find $\Delta = -5.13$ eV and $\Delta = 4.93$ eV for N- and B-doping, respectively, using isolated-atom U values. The corresponding occupancies are $n = 1.71$ and 0.41. If instead effective U values are used, the impurity potentials are $\Delta = -4.06$ eV and $\Delta = 3.70$ eV, respectively, and the occupancies become $n = 1.61$ and 0.51. These results demonstrate that by incorporating self-consistency, the present work expands the applicability of previous nonorthogonal tight-binding models such as Ref. 20.

Having determined the impurity potentials, we can investigate the actual local density of states $L(\omega)$ curves. Of particular importance are the resonances corresponding to donor levels for N-doping and acceptor levels for B-doping. Such resonances are identified as maxima in $L(\omega)$ immediately above or below the Fermi level, respectively. From the plot in Fig. 5, these resonances are easily identified. Here, we have plotted results using the impurity potentials determined above based on isolated-atom U values. To illustrate the rather significant importance of the overlap s due to nonorthogonality, we have, in addition, included curves for s smaller than 0.15. For $s = 0.15$, we find an N donor level of 0.94 eV and a B acceptor level of -0.79 eV, both measured relative to the Fermi level. As s decreases, both of these move away from the Fermi level.
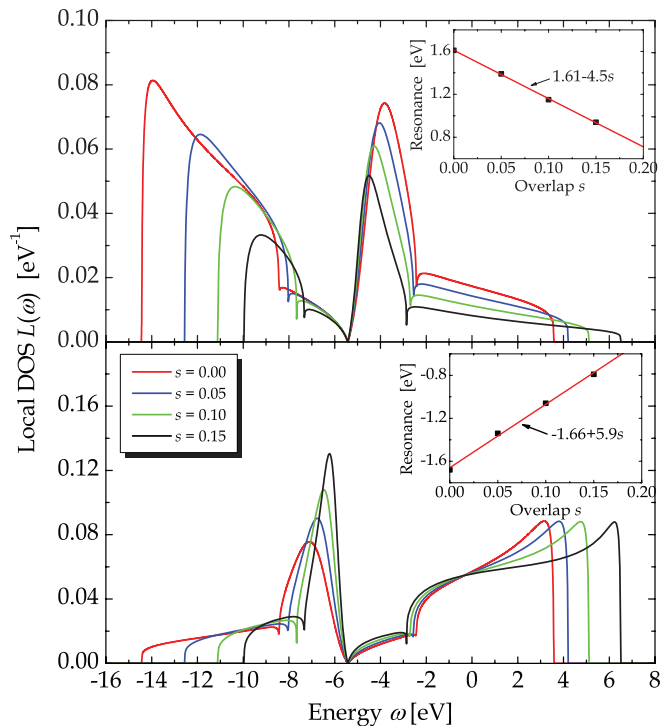
FIG. 5. (Color online) Local density of states (DOS) for N- (top) and B-impurities (bottom). Results for different values of the overlap s are shown. The insets display the s dependence of donor and acceptor resonances, both relative to the Fermi level.

In fact, for $s = 0$, both levels are located almost twice as far from the Fermi level as the original values. This very clearly demonstrates the significance of overlap corrections for an accurate determination of impurity levels.

V. SUMMARY

We have presented an analytical model of impurity levels in graphene and applied it to N- and B-doping. The model incorporates nonorthogonality via nearest-neighbor overlap corrections, and the local density of states on the impurity site is obtained from analytical Green's functions. The impurity potential is subject to a self-consistency condition, which we solve via the impurity occupancy. In this manner, self-consistent impurity potentials for N- and B-dopants have been determined. Our results demonstrate that nonorthogonality has a significant impact on the self-consistent solution. Finally, we have applied this procedure to identify the associated donor and acceptor levels from resonances in the computed impurity density of states.

[1] H. Terrones, R. Lv, M. Terrones, and M. S. Dresselhaus, Rep. Prog. Phys. **75**, 062501 (2012).

[2] A. N. Grigorenko, M. Poline, and K. S. Novoselov, Nature Photon. **6**, 749 (2012).

[3] P. Avouris and F. Xia, MRS Bull. **37**, 1225 (2012).

[4] K. I. Bolotin, K. J. Sikes, J. Hone, H. L. Stormer, and P. Kim, Phys. Rev. Lett. **101**, 096802 (2008).

[5] K. S. Novoselov, A. K. Geim, S. V. Morozov, D. Jiang, Y. Zhang, S. V. Dubonos, I. V. Grigorieva, and A. A. Firsov, Science **306**, 666 (2004).

[6] Z. Jin, J. Yao, C. Kittrell, and J. M. Tour, ACS Nano **5**, 4112 (2011).

[7] D. Usachov, O. Vilkov, A. Grüneis, D. Haberer, A. Fedorov, V. K. Adamchuk, A. B. Preobrajenski, P. Dudin, A. Barinov, M. Oehzelt, C. Laubschat, and D. V. Vyalikh, Nano Lett. **11**, 5401 (2011).

[8] L. Zhao, R. He, K. T. Rim, T. Schiros, K. S. Kim, H. Zhou, C. Gutiérrez, S. P. Chockalingam, C. J. Arguello, L. Pálová, D. Nordlund, M. S. Hybertsen, D. R. Reichman, T. F. Heinz, P. Kim, A. Pinczuk, G. W. Flynn, and A. N. Pasupathy, Science **333**, 999 (2011).

[9] H. Wang, T. Maiyalagan, and X. Wang, ACS Catalysis **2**, 781 (2012).

[10] L. S. Panchakarla, K. S. Subrahmanyam, S. K. Saha, A. Govindaraj, H. R. Krishnamurthy, U. V. Waghmare, and C. N. R. Rao, Adv. Mater. **21**, 4726 (2009).

[11] Y. Fujimoto and S. Saito, Phys. Rev. B **84**, 245446 (2011).

[12] F. Joucken, Y. Tison, J. Lagoute, J. Dumont, D. Cabosart, B. Zheng, V. Repain, C. Chacon, Y. Girard, A. R. Botello-Méndez, S. Rousset, R. Sporken, J.-C. Charlier, and L. Henrard, Phys. Rev. B **85**, 161408 (2012).

[13] Ph. Lambin, H. Amara, F. Ducastelle, and L. Henrard, Phys. Rev. B **86**, 045448 (2012).

[14] V. M. Pereira, J. Nilsson, and A. H. Castro Neto, Phys. Rev. Lett. **99**, 166802 (2007).

[15] T. O. Wehling, A. V. Balatsky, M. I. Katsnelson, A. I. Lichtenstein, K. Scharnberg, and R. Wiesendanger, Phys. Rev. B **75**, 125425 (2007).

[16] A. Lherbier, X. Blase, Y.-M. Niquet, F. Triozon, and S. Roche, Phys. Rev. Lett. **101**, 036808 (2008).

[17] V. M. Pereira, J. M. B. Lopes dos Santos, and A. H. Castro Neto, Phys. Rev. B **77**, 115109 (2008).

[18] S. Wu, L. Jing, Q. Li, Q. W. Shi, J. Chen, H. Su, X. Wang, and J. Yang, Phys. Rev. B **77**, 195411 (2008).

[19] F. M. D. Pellegrino, G. G. N. Angilella, and R. Pucci, Phys. Rev. B **80**, 094203 (2009).

[20] S. Ihnatsenka and G. Kirczenow, Phys. Rev. B **83**, 245442 (2011).

[21] A. Uppstu, K. Saloriutta, A. Harju, M. Puska, and A.-P. Jauho, Phys. Rev. B **85**, 041401 (2012).

[22] M. Elstner, D. Porezag, G. Jungnickel, J. Elsner, M. Haugk, Th. Frauenheim, S. Suhai, and G. Seifert, Phys. Rev. B **58**, 7260 (1998).

[23] J. A. Fürst, T. G. Pedersen, M. Brandbyge, and A.-P. Jauho, Phys. Rev. B **80**, 115117 (2009).

[24] R. Balog, B. Jørgensen, L. Nilsson, M. Andersen, E. Rienks, M. Bianchi, M. Fanetti, E. Lægsgaard, A. Baraldi, S. Lizzit, Z. Sljivancanin, F. Besenbacher, B. Hammer, T. G. Pedersen, P. Hofmann, and L. Hornekær, Nat. Mater. **9**, 315 (2010).

[25] A. Kuc, T. Heine, and G. Seifert, Phys. Rev. B **81**, 085430 (2010).

[26] R. Saito, G. Dresselhaus, and M. S. Dresselhaus, *Physical Properties of Carbon Nanotubes* (Imperial College, London, 1998).

[27] A. Grüneis, C. Attaccalite, L. Wirtz, H. Shiozawa, R. Saito, T. Pichler, and A. Rubio, Phys. Rev. B **78**, 205425 (2008).

[28] M. Gaus, Q. Cui, and M. Elstner, J. Chem. Theory Comput. **7**, 931 (2011).

[29] J. P. Perdew and A. Zunger, Phys. Rev. B **23**, 5048 (1981).

[30] M. Schlüter, M. Rösner, T. O. Wehling, A. I. Lichtenstein, and M. I. Katsnelson, arXiv:1302.1437 (to be published).

[31] T. G. Pedersen, Phys. Rev. B **68**, 245104 (2003).

[32] J. G. Pedersen and T. G. Pedersen, Phys. Rev. B **84**, 115424 (2011).

[33] T. Horiguchi, J. Math. Phys. **13**, 1411 (1972).

[34] T. G. Pedersen, Phys. Rev. B **67**, 113106 (2003).